Morphologies of expansion ridges of elastic thin films onto a substrate

E. A. Jagla
Centro Atómico Bariloche, Comisión Nacional de Energía Atómica, (8400) Bariloche, Argentina
(Received 9 September 2005; revised manuscript received 17 May 2006; published 14 September 2006)

A model of a thin film elastically attached to a rigid substrate is considered. In the case in which the film expands relative to the substrate and assuming certain nonlinear elastic behavior of the film, expansion ridges may appear, in which the material collapses, and the density is higher on average. By studying numerically this process, the possible morphologies of these collapsed regions are presented. They range from circular spots and straight stripes, to wiggle polygonal patterns and ring-shaped domains. The similarity of some of these results with patterns observed in delamination of thin films and biphase epitaxial growth is emphasized.

DOI: 10.1103/PhysRevE.74.036207 PACS number(s): 89.75.Kd, 46.32.+x, 68.55.Jk

I. INTRODUCTION

When the surface of a material contracts with respect to the underlying part, tensile stresses appear in it that can lead to the formation of a crack pattern on the surface [1]. Mud cracking can be considered the prototype of this kind of surface fragmentation phenomenon. The main ingredients of surface fragmentation are a (quasi) two-dimensional film attached to a substrate (I always assume here the substrate is rigid) and a greater expansion of the substrate compared to the film as a function of some external control variable (typically humidity concentration or temperature). The film and substrate can be the same material, as in mud cracks, and in that case it is only a difference in humidity concentration or temperature what identifies film and substrate.

I will concentrate here in a process that in a certain sense is the inverse of surface fragmentation: I consider the film expanding with respect to the substrate. Due to the coupling to the substrate, the greater expansion of the film generates compressive stresses into it. No important effects are expected if the film responds linear elastically to any deformation. If this is the case the film is simply uniformly compressed. But if the film can collapse upon compression, a coexistence of collapsed and noncollapsed regions in the film is expected. The presentation and discussion of the different morphologies of these collapsed regions are the main aim of this paper.

The two main features that fix the morphology of collapsed regions are the degree of mismatch between film and substrate, and the kind of nonlinear elastic behavior of the film, in particular, the characteristics of the collapsed state. Different possibilities are studied here. Most of the results to be presented correspond to the case in which the system is isotropic in the plane of the film (chosen to be the x-y plane), but some results for a model with square symmetry will also be presented. In the next section, I present the model and details of the simulation technique. In Sec. III the main results are presented, and in Sec. IV, I discuss two experimental situations in which the present model can be applied, namely, delamination patterns of thin film and structures appearing during biphase epitaxial growth. Section V contains a summary and conclusions.

II. THE MODEL

The model to be used is an extension of that used in Refs. [2,3] to describe fracture (see also [4,5], where essentially the same technique was originally applied to study a case of martensitic transformations). It considers the film in a two-dimensional approximation as described by the horizontal displacement field $\mathbf{u}(\mathbf{r})$, $\mathbf{r} \equiv (x,y)$. The fundamental variables of the simulations are not the displacements themselves, but the components of the strain tensor. This is defined as

$$\epsilon_{i,j} \equiv \frac{1}{2}\left(\frac{\partial u_i}{\partial x_j} + \frac{\partial u_j}{\partial x_i} + \sum_k \frac{\partial u_k}{\partial x_i}\frac{\partial u_k}{\partial x_j} \right). \tag{1}$$

The quadratic terms guarantee that finite rotations are not present in the strain tensor [6]. In the formalism to be used, the incorporation of these nonlinear terms presents some difficulties. Restricting to low values of the components of the strain tensor, we can use its linear form (usually called the infinitesimal, or Cauchy strain tensor), namely

$$\varepsilon(i,j) \equiv \frac{1}{2}\left(\frac{\partial u_i}{\partial x_j} + \frac{\partial u_j}{\partial x_i} \right). \tag{2}$$

Typically, strains up to a few percents and rotations of up to a few degrees can be accurately described using the linear strain tensor, and I will assume this is the case in all results presented below. For convenience, instead of ε_{ij} I will use the following variables:

$$e_1 \equiv (\varepsilon_{11} + \varepsilon_{22})/2,$$

$$e_2 \equiv (\varepsilon_{11} - \varepsilon_{22})/2,$$

$$e_3 \equiv \varepsilon_{12} = \varepsilon_{21}. \tag{3}$$

These three variables are not independent. They satisfy the St. Venant compatibility constraint [4,5,7], which reads

$$(\partial_x^2 + \partial_y^2)e_1 - (\partial_x^2 - \partial_y^2)e_2 - 2\partial_x\partial_y e_3 = 0. \tag{4}$$

The model will be defined by giving the form of the free energy density of the system in terms of the variables e_1, e_2, and e_3. The free energy contains three terms: a local term f_0, a gradient term f_∇, and a substrate interaction term f_{subs}. The existence of a collapse transition for the film is encoded in the form of the local free energy term f_0. If we intend to describe a material that is isotropic in the x-y plane, only rotationally invariant combinations of the basic variables e_i should enter the free energy. Those that can be constructed

 ©2006 The American Physical Society

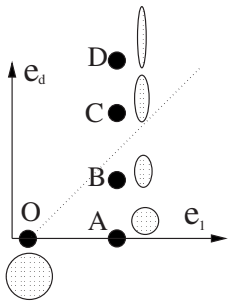

FIG. 1. Different possibilities for the location of the collapsed minimum in the e_1-e_d plane. The elastic minimum is located at O. The sketches show qualitative (in the plane of the system, namely, the x-y plane) an originally circular piece of material at O and its collapsed form for different locations of the collapsed minimum. In cases A and B (i.e., below the dotted line) an original circular piece of material contracts in all directions, whereas for C and D there is a direction in which it actually expands. Note that the orientation of the ellipses is arbitrary in the x-y plane; all orientations produce the same e_d, and thus the same energy.

from the e_i's are e_1 itself, and $e_d \equiv \sqrt{e_2^2+e_3^2}$. A perfectly elastic material is described by a local free energy having a quadratic minimum, namely its local free energy is of the form

$$f_0^{elastic} = B(e_1 - e_1^0)^2 + \mu(e_2^2 + e_3^2), \tag{5}$$

where B and μ are, respectively, proportional to the bulk and shear modulus of the material. With the present choice, in a completely relaxed state the system has $e_1 = e_1^0$, $e_2 = e_3 = 0$.

If the material can collapse, f_0 must have nonquadratic terms and have some other minimum at some e_1^C, e_d^C describing the collapsed state. For the description in terms of the linear strain tensor to be accurate, we must require $|e_1^C - e_1^0| \ll 1$ and $e_d^C \ll 1$. The position of the collapsed minimum [in particular, the ratio $\nu \equiv e_d^C/(e_1^C - e_1^0)$] will have important consequences on the morphologies of the collapsed regions that will be observed. Different locations of the collapsed minimum will be explored and discussed here. They are qualitatively depicted in Fig. 1 as cases A, B, C, and D. It is necessary to point out that the change in morphologies that will be observed among different cases is rather smooth; the distinction is made for classification purposes only. I have observed in the numerical simulations that in most cases the morphologies of the collapsed patterns depend only on the position of the collapsed minimum with respect to the elastic minimum, the detailed form of f_0 being of minor importance. Only in case A, there are noticeable variations depending on the value of the shear modulus of the collapsed state μ^C with respect to the value in the normal state μ. Thus, in this case, two subcases will be distinguished: A1, in which μ^C is greater or equal to μ, and A2, in which μ^C is lower than μ. Note that when the collapsed state has $e_d^C \neq 0$, it corresponds actually to a ring of minima in the e_1, e_2, e_3 space. In other words, the collapse of a circular piece of material to a state with $e_d \neq 0$ produces an ellipse, but this ellipse in the x-y plane can be in any orientation. The crucial features of each f_0 used in the simulations, mainly the position of the free energy minima, are indicated on each figure below. As other details of the f_0 part of the free energy are not crucial for the results, the exact form of f_0 in all the cases A–D is given in the Appendix.

Gradient terms in the free energy will be taken in the form

$$f_{\nabla} = \sum_{i=1,2,3} \alpha_i (\nabla e_i)^2, \tag{6}$$

where $\alpha_2 = \alpha_3 \equiv \alpha$ should be chosen to retain rotational invariance. In all results below I take for simplicity also $\alpha_1 = \alpha$. Some additional runs in cases with $\alpha_1 \neq \alpha$ show that the results are not crucially dependent on this choice.

The elastic interaction with the substrate is easily written in terms of the displacement variables $\mathbf{u}$:

$$f_{subs} = \frac{\gamma}{2}|\mathbf{u}(\mathbf{r})|^2, \tag{7}$$

where γ measures the stiffness of this interaction. As I take the components of ε to be the basic variables, this energy has to be recast in terms of them. This is more easily done in the Fourier space, and the result can be easily written after an integration over the whole system as

$$\int d^2 r f_{subs} = 2\gamma \int' d^2 k \frac{|\tilde{e}_2(\mathbf{k})|^2 + |\tilde{e}_3(\mathbf{k})|^2}{k^2}, \tag{8}$$

where $\tilde{e}_i(\mathbf{k})$ are the Fourier transforms of the original $e_i(\mathbf{r})$, and the prime in the integral indicates that the $k=0$ mode is excluded. To avoid a divergent energy contribution, the value of $\tilde{e}_1(\mathbf{k}=0) = \bar{e}_1$ (where the bar notes the spatial average) has to be adjusted for the system to fit on average onto the substrate, namely, the mismatch with the substrate is incorporated in the model precisely through the value given to $\bar{e}_1$.

Nontrivial spatial patterns originate in the existence of different minima of the free energy f_0. The typical spatial scale of these patterns is governed by a competition between gradient and substrate terms. In fact, in Fourier space a spatial oscillation of the e's of wave vector $\sim k$ and amplitude A produces a contribution to the energy density of the order of $\alpha A^2 k^2$ from the gradient terms, and $\gamma A^2/k^2$ from the substrate term. The sum of these two contributions has a minimum at a value of k of the order of $(\gamma/\alpha)^{1/4}$. This is the order of magnitude of the main spatial variations that will be seen to appear in the simulations.

The equations of motion are taken to be of the overdamped form, namely

$$\frac{\partial e_i}{\partial t} = -\lambda \frac{\delta F}{\delta e_i} \quad (i = 1,2,3), \tag{9}$$

where

$$F = \int d^2 r (f_0 + f_{\nabla} + f_{subs}). \tag{10}$$

The Saint Venant constraint is implemented by the use of Lagrange multipliers. Full details can be seen in [2,5].

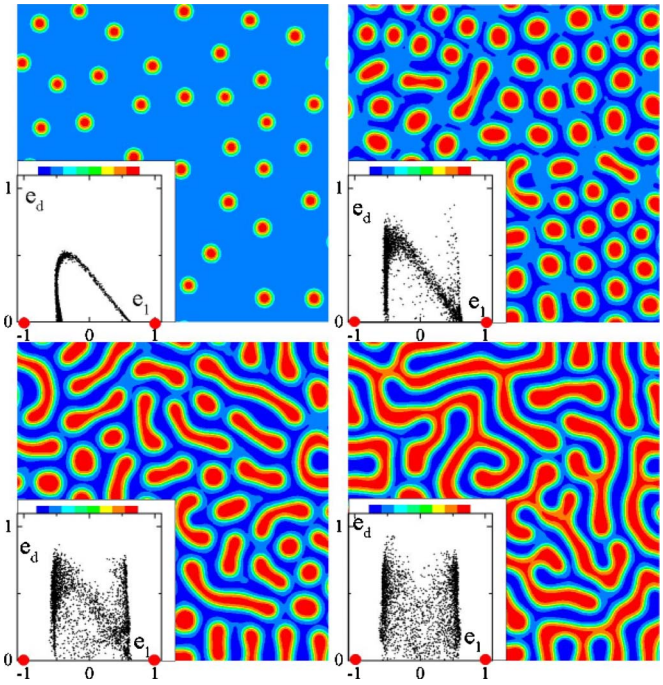

FIG. 2. (Color online) Spatial configurations obtained for case A1, for values of $\bar{e}_1$ equal to −0.4, −0.2, −0.1, and 0 (from left to right and from top to bottom). The shadows indicate values of e_1, with the scale indicated in the inset. In the inset plots, the distribution of e_d vs e_1 is shown for all elements of the system. The positions of the minima of the local free energy are indicated by the two circles in each inset. In the present case the shear modulus of the intact and collapsed phases coincide, namely $\mu=\mu^C$. See the full expression for the local free energy in the Appendix.

III. RESULTS

For each set of parameters and any given initial condition, the system evolving according to Eq. (9) will settle down in a configuration that minimizes (albeit locally) the total energy F. We will see that, in general, metastable states appear very often in the simulations. In order to get as close as possible to the true ground state configuration, an annealing process was implemented in which a stochastic term was added to the right-hand side of Eq. (9), and the intensity of this term was progressively reduced down to zero during the simulation. The results shown are the final configuration of the annealing process, and are good examples of the typical morphologies favored by the competition of the different energy terms.

Results will be presented for a unique set of values of the coefficients α and γ in the gradient and substrate interaction terms [Eqs. (6) and (8)]. It can be shown that a change of these parameters can be absorbed in a rescaling of the spatial coordinate and a global redefinition of the free energy [8]. I have chosen the values $\alpha=3$, $\gamma=0.01$, for which the expected spatial scale of the structures to be seen (based on the estimation in the previous section) is of the order of ten mesh parameters. Thus, the geometrical features of the patterns will be reasonably larger than the discretization of the numerical mesh, and this is appropriate to eliminate spurious effects associated with this discreteness.

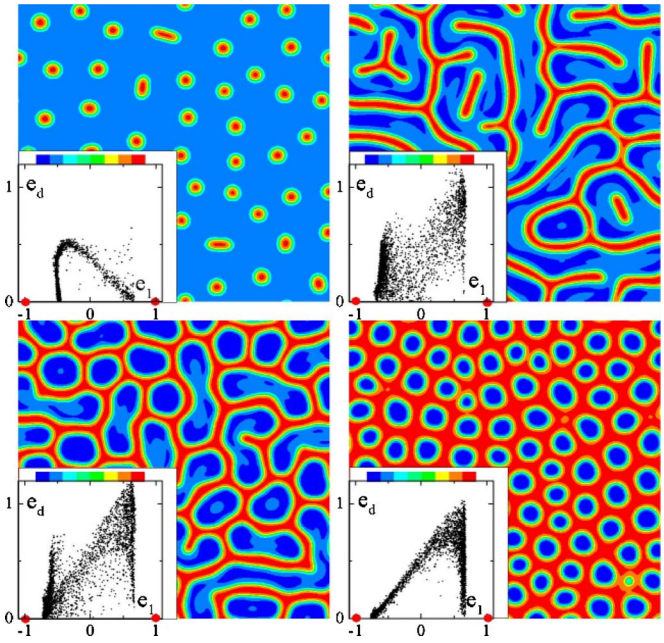

FIG. 3. (Color online) Same as Fig. 2 but for case A2, and values of $\bar{e}_1$ of −0.4, −0.2, −0.1, and 0.2. In the present case $\mu/\mu^C \sim 100$.

Before presenting the configurations, it is important to clarify the meaning that will be given to the overall values of the e's. As already stated, neglecting the quadratic terms in the full strain tensor means that the description will be accurate if all e's are small. I take the values of the e's in the plots and in the expression in the Appendix to be scaled values, the true values will be supposed to be given by a constant factor r times the scaled values. If r is taken progressively smaller, the present description becomes progressively more accurate. With this consideration in mind, we can now look at the configurations obtained, as depicted in Figs. 2–6, corresponding to cases A–D, respectively. Each panel in each figure represents a different value of $\bar{e}_1$, i.e., a different degree of mismatch with the substrate. Each main plot shows the spatial distribution of e_1 or e_d (depending on which is more representative in each case). The scale for this plot is indicated in the bar of the inset. The inset also shows the combined distribution of e_d vs e_1 for all elements in the system. I now discuss separately each case.

Case A in which the collapsed minimum is isotropic (i.e., it has $e_d^C=0$) can be appropriately called a volume collapse transition. In the absence of a substrate interaction, this case has been extensively studied, for instance, in Refs. [9–11] in the context of phase separation in alloys. In that case there is a coarsening of the spatial structures obtained, that grow in size as time evolves. In our case in which a substrate interaction is present, the spatial structures observed stabilize with a well-defined typical spatial scale, given by the competition between gradient and substrate terms of the free energy, as explained in the previous section: too small patterns are discouraged by a large gradient energy, whereas too large patterns pay too much substrate interaction energy.

When the collapsed phase has the same shear modulus than the original phase (Fig. 2) the results can be compared,

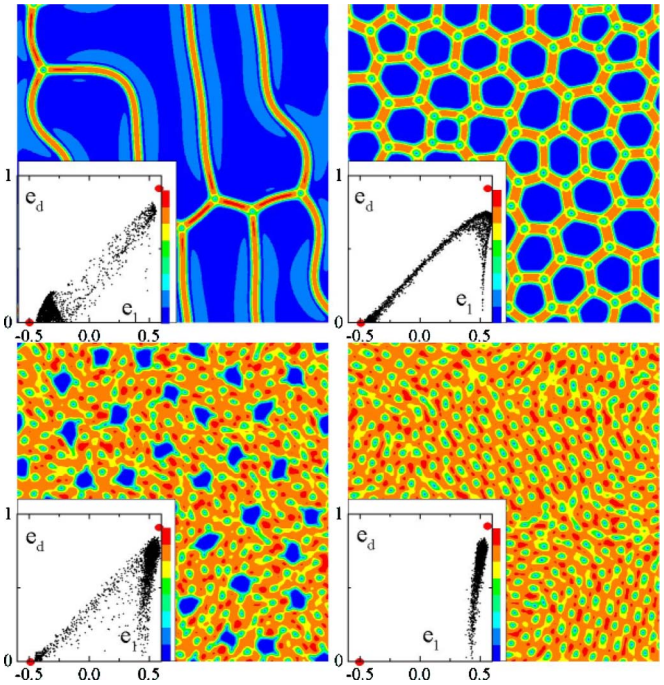

FIG. 4. (Color online) Same as Fig. 2 but for case B, and values of $\bar{e}_1$ of −0.2, 0, 0.4, and 0.5 (note that in this and next two figures, the main plot shows values of e_d, instead of e_1).

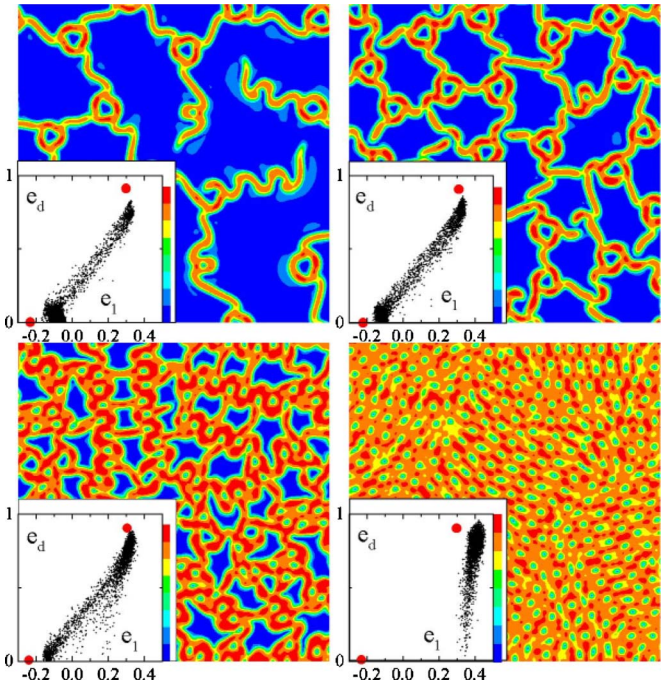

FIG. 6. (Color online) Same as Fig. 4 but for case D, and values of $\bar{e}_1$ of −0.005, 0.05, 0.2, and 0.4.

for instance, to those in Ref. [10], Figs. 2(a) and 2(b). The main difference is that those in Ref. [10] are patterns that are coarsening, while ours are stable due to the substrate interaction, but they look qualitatively similar.

In the case in which the collapsed phase has a lower shear modulus than the original phase (case A2, Fig. 3), bubbles of the softer phase tend to be unstable with respect to elongation [9,11]. This is clear, in particular, comparing the second panels in Figs. 2 and 3. Note that the effect is not symmetric: if the mismatch is such that the minority phase corresponds to the more rigid phase, then the bubbles remain stable (compare panels with $\bar{e}_1=-0.2$ and $\bar{e}_1=0.2$ in Fig. 3). Patterns similar to these can be seen in Ref. [10], Fig. 2, (i) and (j). In both cases A1 and A2, for even larger mismatch (not shown) all the system becomes uniformly collapsed, with $e_1(\mathbf{r})=\bar{e}_1$, $e_2(\mathbf{r})=e_3(\mathbf{r})=0$. I will not analyze case A in more detail since, as mentioned, it has been analyzed in detail in qualitatively similar situations.

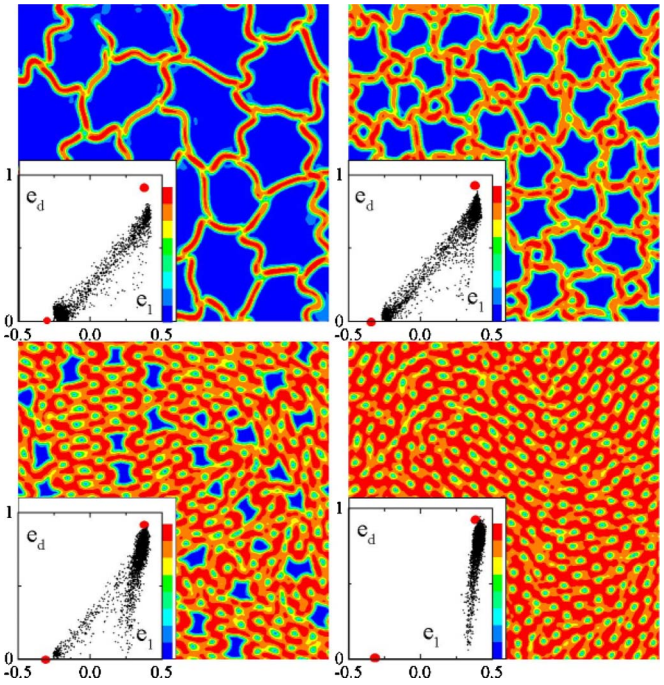

FIG. 5. (Color online) Same as Fig. 4 but for case C, and values of $\bar{e}_1$ of −0.05, 0.1, 0.3, and 0.4.

Cases in which the collapsed minimum has nonzero e_d^C have not been analyzed before, to my knowledge, and are the main contribution of the present paper. Starting with case B (Fig. 4) we observe a stronger tendency to form stripes and polygonal patterns than in the previous cases. There is also an important difference with case A for large mismatch (lower-right panel): Now each elemental piece of the system prefers to be as close as possible to the collapsed minimum, that locates at a nonzero value of e_d. However, not all elements can have the same values of e_2 and e_3, since the spatial averages $\bar{e}_2$ and $\bar{e}_3$ should be zero. The existence of the substrate also discourages uniform phases with constant e_2 or e_3. The configuration of the system is such that individual elements tend to be distributed close to the ring of minima in the e_2-e_3 plane. In real space, singularities appear at which $e_2=e_3=0$, and around them the configuration point in the e_2-e_3 plane rotates 2π, clockwise, or counterclockwise, thus defining "vortexlike" or "antivortexlike" defects. Typical distance between these defects is again controlled by $(\alpha/\gamma)^{1/4}$, fixed by the competition between gradient and substrate terms. In particular, the density of these defects tends to zero for vanishing substrate interaction.

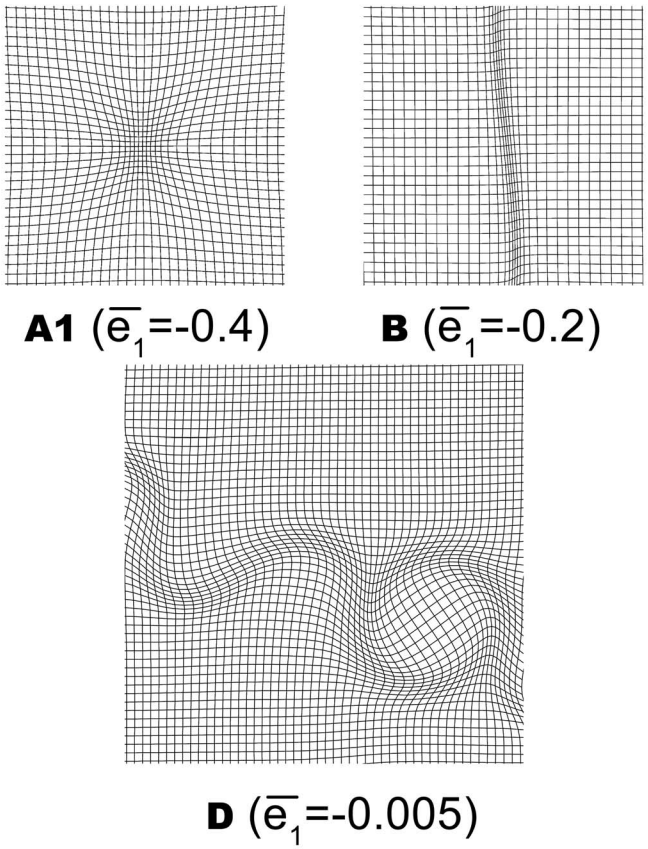

FIG. 7. Detailed structure of the lattice in particular sectors of Figs. 2, 4, and 6. I plot the numerical (square) mesh shifted by the corresponding displacement field **u**. For visualization reasons the displacement field **u** has been appropriately increased by a constant factor.

Cases C and D (Figs. 5 and 6) present an interesting difference in morphology with respect to previous cases: Stripes of collapsed regions have now a wavy structure. In some cases, we observe even the existence of ring-shaped collapsed regions. The origin of wiggling collapsed stripes and rings is dictated by the tendency of the model to minimize the energy. A closer look to the configurations clarifies the way in which circular or wiggle patterns are able to reduce the total energy. I refer first of all to Fig. 7, where some special parts of the patterns found in the simulations are shown in more detail. In this figure I plot the actual position of the nodes of the numerical mesh, namely the displacement field $\mathbf{u}(\mathbf{r})$ (this is obtained from the e's by numerical integration). For comparison, the structure of a circular and striped collapsed region in cases A and B, and a ring and a piece of a wiggled striped in case D are shown. The structures in cases A and B, show that the displacement field **u** is radial in the case of a circular spot, or perpendicular to the axis in the case of a stripe. Starting from these configurations, we can understand how the energy is reduced in case C and D as follows: First of all, note that cases C and D correspond to situations in which the collapse of a circular piece of material generates an ellipse with the major axis larger than the original diameter of the circle, while it was smaller in cases A and B (see Fig. 1). In other words, these cases have $\nu > 1$. Analyzing the configuration of a ring in Fig. 7(c), we can see that the center is rotated (the rotation sense is arbitrary) thus generating a finite shear in an annular region. This shear increases e_d, thus reducing the energy if the collapsed minimum has a sufficiently large ν. In addition, upon this rotation, the central region is able to expand, getting closer to the noncollapsed minimum, and reducing the energy further. For the wiggle pattern, we can consider it as a deformation of the straight stripe. The scheme of this process is depicted in Fig. 8. First of all note that for the linear stripe and in the case in which $\nu > 1$, the collapsed stripe is longitudinally compressed. The wiggling geometry is just a way of relaxing this compression: once the stripe is undulated, regions near the maxima of the undulation in Fig. 8 can expand in the longitudinal
direction, thus relaxing to a more favorable configuration.

IV. PRACTICAL REALIZATIONS

I have analyzed the situation of a material that has two well-defined elastic configurations of minimum energy. We have seen that nontrivial morphologies may appear when a quasi-two-dimensional piece of such a material is uniformly attached to a rigid substrate. In searching for practical realizations, it will be difficult to find that all the assumptions in the model are satisfied, however, it can be a good idealized case to study some practical problems. Two examples will be presented now.

The first case corresponds to the patterns observed in delamination of thin films [12–14]. In this case, typically, a film is grown onto a substrate, and due to chemical differences between substrate and film (which may be enhanced by temperature changes) elastic stresses develop between them. If the stresses are compressive within the film, they may induce the buckling up of part of the film, giving rise to patterns that have been termed "telephone-cord"-like, due to their wavy appearance. In some cases, wavy polygonal patterns of buckled regions are observed, remarkably similar to those in Figs. 5 and 6 [see, in particular, Fig. 1(a) in Ref. [13]].

The microscopic equations governing the delamination process are the Foppl-Von Karman equations [14]. They model the three-dimensional displacement of the points of the buckled film. It seems unlikely that this set of nonlinear equations can be simply mapped to the model presented here. However, the similarity of the patterns observed in the two cases does not seem to be fortuitous, and in fact, a qualitative relation between the two models can be made.

A stripe of buckled material is qualitatively depicted in Fig. 9(a). On the stripe, the film has detached from the substrate, and the compressive stress on the film has been partially released due to the expansion of the film in the direction perpendicular to the stripe allowed by the buckling. This configuration is the counterpart of a stripe of collapsed material in the model I have presented here [Fig. 9(b)]. In both cases there are two qualitatively different configurations corresponding to two different minima of the energy: the attached and unbuckled film, that parallels the isotropic minimum of our model, and the detached and buckled film,

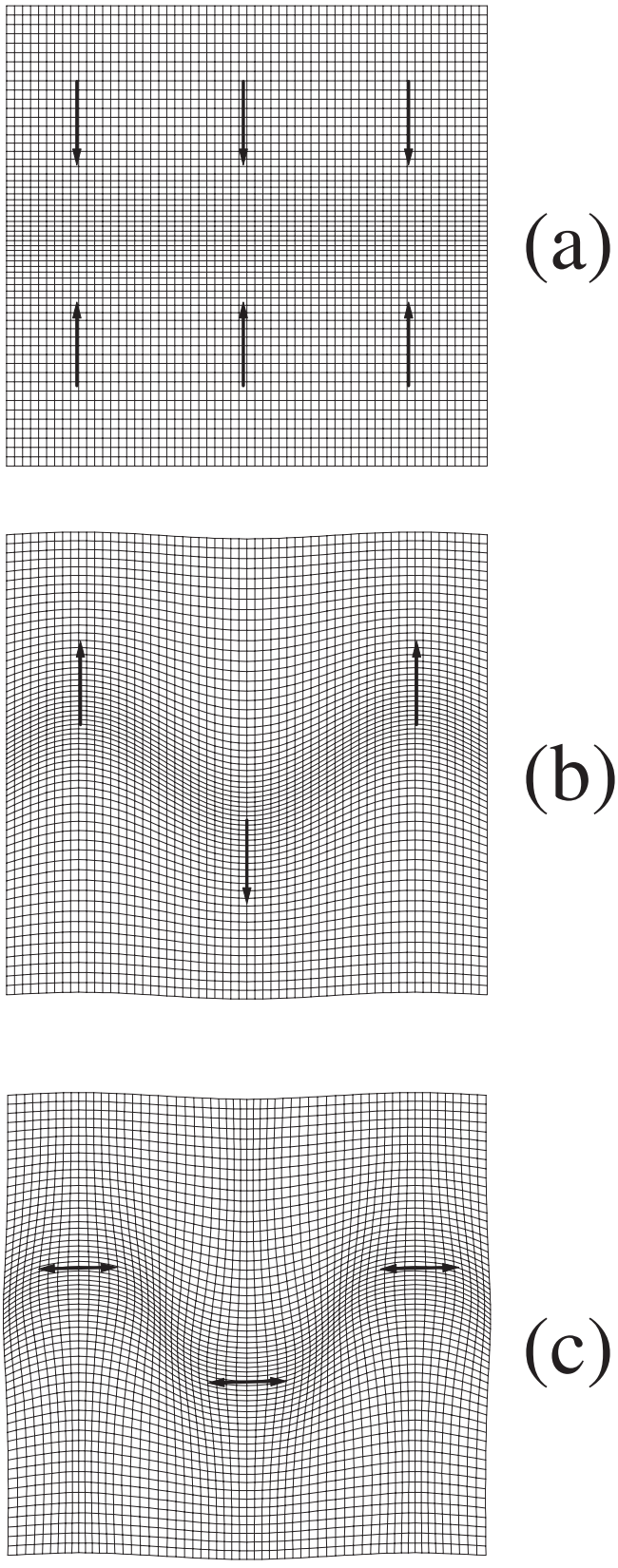

FIG. 8. Schematic displacement field $\mathbf{u}(\mathbf{r})$ for a stripe of collapsed region (a), the same stripe undulated through a sinusoidal perturbation (b), and the relaxation of the longitudinal stress that allows the system to reduce the energy and stabilize the wiggling pattern (c).

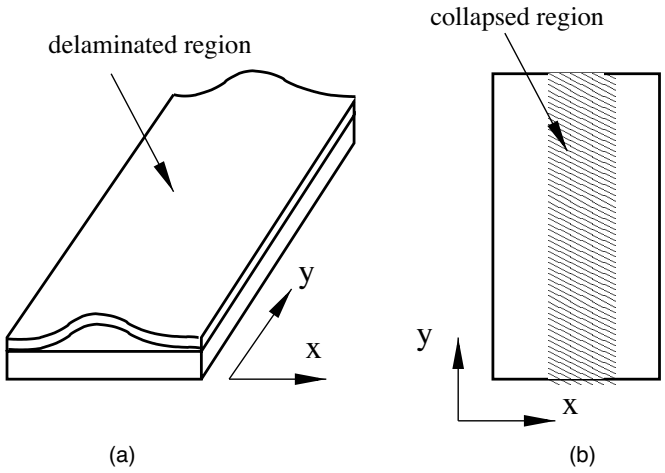

FIG. 9. A stripe of delaminated thin film (a), and the qualitative equivalent as a region of collapsed material in our model (b).

which is represented by the collapsed minimum of the model. The additional crucial analogy between the two cases that justifies the similarity of the patterns is the following: In the present model for sufficiently large ν, I have already indicated how the undulation of the collapsed region is able to reduce the energy of the system. Exactly the same analysis is valid for the buckling film. In fact, a stripe of buckled film is longitudinally compressed, and the undulation of the stripe is able to release part of this elastic energy. This qualitative explanation of undulations of buckled stripes was noticed in the literature [14]. This analysis allows us to understand why the two problems present notably similar morphologies of patterns. I want to point out that the other characteristic morphology that appears in the collapse model, namely the ring-shaped collapsed region, has also been occasionally observed in delamination, see Ref. [13], Fig. 2(a). All these similarities might point to a deeper correspondence between the two models. How this correspondence would come out is not clear to me at the moment, but is worthy of further investigation.

A second problem to which the present model can be applied is the epitaxial growth of competing phases with different crystallographic parameters [15]. In this problem, two (or more) chemically different phases compete to grow epitaxially onto a substrate. If the growing is coherent (namely, if no dislocations appear in the crystalline structure), elastic stresses are accumulated during growth, and which phase is preferred locally to grow the material is dictated by the tendency to minimize the total elastic energy of the system. Then typically spatial patterns formed by the coexistence of the different phases are observed. This situation can be appropriately modeled with the present formalism just thinking on the two minima of the free energy of the model as describing the two different growing phases, rather than describing two different states of a single phase. To reasonably describe this situation, one of the previously used assumptions needs to be changed: Epitaxy is strongly dependent on the crystalline structures of the phases, and isotropy of the model in the x-y plane is not justified. However, the model can be easily modified to account for anisotropies in

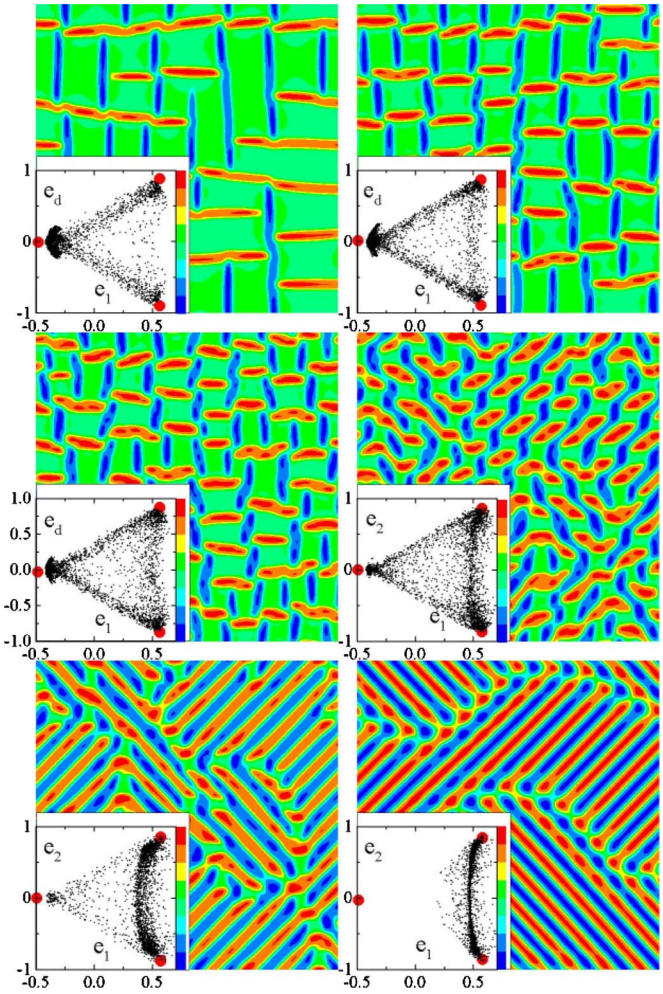

FIG. 10. (Color online) Morphologies for an anisotropic case in which the collapsed minima are located at $e_2=\pm e_2^C$, $e_3=0$. The values of $\bar{e}_1$ for the plots are –0.1, 0, 0.1, 0.3, 0.4, and 0.5, respectively. Note that as long as there is some fraction of the system in the isotropic elastic minimum (first three plots) the morphology of the collapsed regions is that of intercrossed stripes along x and y, while when the fraction of the system in the elastic configuration is negligible (last two plots) the morphology changes to stripes along the diagonals.

the x-y plane. I will present here only an example of the possible outcome obtained using an anisotropic free energy. Let us consider that the substrate has a square symmetry (assumed to be aligned with the x-y coordinate axis), that one of the growing phases has also a square symmetry with a larger unit cell than the substrate, and that the second growing phase has a rectangular symmetry with a lower unit cell volume than that of the substrate. This situation corresponds to a local free energy f_0 having an elastic minimum as usual, and a collapsed minimum localized now at $e_2=\pm e_2^C$, $e_3=0$. In this way the ring of minima in the e_2-e_3 plane of the previous cases is replaced by a couple of minima. The exact form of f_0 I use is given in the Appendix. The morphologies obtained are shown in Fig. 10. As expected, the existence of a rectangular phase reflects clearly on the morphology of the patterns. Note how upon change of the fraction of the rectangular phase (which is dictated, as usual, by the degree of mismatch with the substrate), the morphology changes from stripes of rectangular phase parallel to the axis (for low density of rectangular phase), to stripes of rectangular phase along the diagonals (for the case of a large fraction of the rectangular phase) [16].

V. SUMMARY AND CONCLUSIONS

Expansion ridges are analog to surface cracks, with the difference that they appear when a film expands with respect to the substrate (contrary to cracks, that appear when the film contracts with respect to the underlying material). A nonlinear elastic behavior of the film, namely the possibility of a collapse upon applied stress, is necessary for expansion ridges to appear. I have simulated expansion ridges through an elastic model that uses the components of the strain tensor as fundamental variables. I have shown how complex morphologies can appear due to competitive elastic interactions in the system. By changing the parameters of the model, collapsed regions in the form of bubbles, straight stripes, undulating stripes, and rings have been obtained. I have argued that the model can be applied to understand the characteristics of delamination patterns in thin films, and biphase epitaxial growth. I have concentrated in the description of the morphologies, and then the presentation has been qualitative to a large extent. A few important things can be highlighted: The relevant spatial scale of the patterns is seen to be fixed by a competition between an interaction with the substrate and gradient effects. In the case in which the collapse is isotropic, well-known results in the field of alloy decomposition have been reproduced. Wiggle stripes of collapsed material appear when the collapse of an elemental circular piece of material is such that contraction in one direction is accompanied by expansion in the perpendicular direction. A comparison has been made between these wiggling patterns and those observed in delamination of thin films. I have also provided an example showing that anisotropy can be easily incorporated in the model, and showed that the anisotropic case may have relevance for the study of biphase epitaxial growth. More detailed studies an comparisons on each of these individual realizations are in progress.

APPENDIX

I give here the explicit expressions for the local free energy f_0 used in each of the simulations presented in the paper. For Figs. 2 and 3, I use

$$f_0=\left[\frac{e_d^2}{2}+(e_1-1)^2\right]\left[1+\tanh(3e_1)\right]+\left[C_1\frac{e_d^2}{2}+(e_1+1)^2\right]\times\left[1-\tanh(3e_1)\right] \tag{A1}$$

with $C_1=1$ in Fig. 2, and $C_1=0$ in Fig. 3. In Figs. 4–6, I use

$$f_0=\left[\frac{e_d^2}{2}+\frac{e_d^4}{4}+(e_1-C_3)^2\right]\left[1+\tanh(C_2e_1)\right]+\left[-\frac{e_d^2}{2}+\frac{e_d^4}{4}+(e_1+C_3)^2+\frac{1}{4}\right]\left[1-\tanh(C_2e_1)\right] \tag{A2}$$

with $C_2=2$ and $C_3=0.4$ in Fig. 4; $C_2=3.5$ and $C_3=0.2$ in Fig. 5; and $C_2=4$ and $C_3=0.1$ in Fig. 6. Finally, in Fig. 10 I use

$$f_0 = \left[\frac{e_2^2}{2} + \frac{e_2^4}{4} + (e_1 - C_3)^2\right]\left[1 + \tanh(C_2 e_1)\right] + \left[-\frac{e_2^2}{2} + \frac{e_2^4}{4} + (e_1 + C_3)^2 + \frac{1}{4}\right]\left[1 - \tanh(C_2 e_1)\right] + e_3^2 \tag{A3}$$

with $C_2=2$ and $C_3=0.4$.

The equilibrium phases of the system correspond to the minima of these expressions. For instance, in the case of Figs. 2 and 3 the minima are located at $e_1 \simeq -1.022$, $e_2=e_3=0$ (the "normal state") and $e_1 \simeq 1.022$, $e_2=e_3=0$ (the "collapsed state"). The elastic parameters of the different states (such as bulk and shear modulus) can be evaluated calculating the appropriate curvature of the free energy f_0 at the corresponding minimum.

[1] K. Leung and J. V. Andersen, Europhys. Lett. **38**, 589 (1997); S. Kitsunezaki, Phys. Rev. E **60**, 6449 (1999); A. Groisman and E. Kaplan, Europhys. Lett. **25**, 415 (1994); P. Meakin, Science **252**, 226 (1991); W. Korneta, S. K. Mendiratta, and J. Menteiro, Phys. Rev. E **57**, 3142 (1998); K. A. Shorlin, J. R. de Bruyn, M. Graham, and S. W. Morris, *ibid.* **61**, 6950 (2000); T. Hornig, I. M. Sokolov, and A. Blumen, *ibid.* **54**, 4293 (1996); K. T. Leung and Z. Neda, Phys. Rev. Lett. **85**, 662 (2000).

[2] V. I. Marconi and E. A. Jagla, Phys. Rev. E **71**, 036110 (2005).

[3] E. A. Jagla, Phys. Rev. E **69**, 056212 (2004).

[4] S. Kartha, J. A. Krumhansl, J. P. Sethna, and L. K. Wickham, Phys. Rev. B **52**, 803 (1995).

[5] S. R. Shenoy, T. Lookman, A. Saxena, and A. R. Bishop, Phys. Rev. B **60**, R12537 (1999); T. Lookman, S. R. Shenoy, K. O. Rasmussen, A. Saxena, and A. R. Bishop, *ibid.* **67**, 024114 (2003).

[6] L. D. Landau and E. M. Lifshitz, *Theory of Elasticity* (Oxford, Pergamon Press, 1970).

[7] D. Chandrasekharaiah and L. Debnath, *Continuum Mechanics* (Academic Press, San Diego, 1994).

[8] E. A. Jagla, Phys. Rev. E **70**, 046204 (2004).

[9] C. Sagui and R. C. Desai, Phys. Rev. Lett. **71**, 3995 (1993); Phys. Rev. E **49**, 2225 (1994); **52**, 2807 (1995).

[10] D. Orlikowski, C. Sagui, A. Somoza, and C. Roland, Phys. Rev. B **59**, 8646 (1999).

[11] A. Onuki, *Phase Transition Dynamics* (Cambridge University Press, Cambridge, 2002).

[12] J. Colin, F. Cleymand, C. Coupeau, and J. Grilhé, Philos. Mag. A **80**, 2559 (2000); F. Cleymand, C. Coupeau, and J. Grilhé, Scr. Mater. **44**, 2623 (2001); M.-W. Moon, H. M. Jensen, J. W. Hutchinson, K. H. Oh, and A. G. Evans, J. Mech. Phys. Solids **50**, 2355 (2002); M.-W. Moon, K.-R. Lee, K. H. Oh, and J. W. Hutchinson, Acta Mater. **52**, 3151 (2004).

[13] C. Coupeau, Thin Solid Films **406**, 190 (2002).

[14] B. Audoly, Phys. Rev. Lett. **83**, 4124 (1999); K. M. Crosby and R. M. Bradley, Phys. Rev. E **59**, R2542 (1999); P. Peyla, *ibid.* **62**, R1501 (2000); F. Cleymand, J. Colin, C. Coupeau, and J. Grilhé, Eur. Phys. J.: Appl. Phys. **17**, 173 (2002).

[15] H. Zheng, J. Wang, S. E. Lofland, Z. Ma, L. Mohaddes-Ardabili, T. Zhao, L. Salamanca-Riba, S. R. Shinde, S. B. Ogale, F. Bai, D. Viehland, Y. Jia, D. G. Schlom, M. Wuttig, A. Roytburd, and R. Ramesh, Science **303**, 661 (2004); J. Li, I. Levin, J. Slutsker, V. Provenzano, P. K. Schenck, R. Ramesh, J. Ouyang, and A. L. Roytburd, Appl. Phys. Lett. **87**, 072909 (2005); A. Artemev, J. Slutsker, and A. L. Roytburd, Acta Mater. **53**, 3425 (2005).

[16] It is worth noticing that the present case can also be interpreted in the context of a model recently introduced to describe a square-to-rectangular martensitic transformation [4,5]. In fact, we can consider the isotropic minimum as representing the austenite phase, and the collapsed minima as the martensite phase, in its two different variants: $e_2=\pm e_2^C$. In the case of Refs. [4,5] (in which a substrate has not been included), volume change during martensitic transformation is assumed to be negligible, and a phase of diagonal stripes similar to that in the lower plots of Fig. 10 has been observed [4,5] (note that in our case the width of the diagonal stripes is fixed by the strength of the interaction with the substrate). From the results of the first plots of Fig. 10 we can conclude that a phase of stripes along the x and y directions is favored instead when the transformation has an appreciable volume change and a finite fraction of the austenite phase remains in the system.